



Indentation-Induced Structural Changes in Vitreous Silica Probed by *in-situ* Small-Angle X-Ray Scattering

Sindy Fuhrmann^{1,2*}, Guilherme N. B. M. de Macedo¹, René Limbach¹, Christina Krywka^{3,4}, Sebastian Bruns⁵, Karsten Durst⁵ and Lothar Wondraczek¹

¹ Otto Schott Institute of Materials Research, Friedrich Schiller University Jena, Jena, Germany, ² Institute of Ceramic, Glass and Construction Materials, TU Bergakademie Freiberg, Freiberg, Germany, ³ Institute of Materials Research, Helmholtz-Zentrum Geesthacht, Outstation at DESY, Geesthacht, Germany, ⁴ Institute of Experimental and Applied Physics, Christian Albrechts University, Kiel, Germany, ⁵ Physical Metallurgy, TU Darmstadt, Darmstadt, Germany

The transient (or permanent) structural modifications which occur during local deformation of oxide glasses are typically studied on the basis of short-range data, for example, obtained through vibrational spectroscopy. This is in contrast to macroscopic observations, where variations in material density can usually not be explained using next-neighbor correlations alone. Recent experiments employing low-frequency Raman spectroscopy have pointed-out this issue, emphasizing that the deformation behavior of glasses is mediated through structural heterogeneity and drawing an analogy to granular media. Here, we provide additional support to this understanding, using an alternative experimental method. Structural modification of vitreous silica in the stress field of a sharp diamond indenter tip was monitored by *in-situ* small-angle X-ray scattering. The influenced zone during loading and after unloading was compared, demonstrating that changes in the position of the first sharp diffraction peak (FSDP) directly in the center of the indent are of permanent character. On the other hand, variations in the amplitude of electron density fluctuations (AEDF) appear to fully recover after load release. The lateral extent of the modifications and their relaxation are related to the short- to intermediate-range structure and elastic heterogeneity pertinent to the glass network. With support from Finite Element Analysis, we suggest that different structural length scales govern shear deformation and isotropic compaction in vitreous silica.

Keywords: *in-situ* indentation, SAXS, vitreous silica, glass, heterogeneity, density fluctuation, densification

OPEN ACCESS

Edited by:

Randall Youngman,
Corning Inc., United States

Reviewed by:

Liping Huang,
Rensselaer Polytechnic Institute,
United States
Ling Cai,
Corning Inc., United States

*Correspondence:

Sindy Fuhrmann
sindy.fuhrmann@ikgb.tu-freiberg.de

Specialty section:

This article was submitted to
Ceramics and Glass,
a section of the journal
Frontiers in Materials

Received: 12 February 2020

Accepted: 11 May 2020

Published: 09 June 2020

Citation:

Fuhrmann S, de Macedo GNBM,
Limbach R, Krywka C, Bruns S, Durst
K and Wondraczek L (2020)
Indentation-Induced Structural
Changes in Vitreous Silica Probed by
in-situ Small-Angle X-Ray Scattering.
Front. Mater. 7:173.
doi: 10.3389/fmats.2020.00173

INTRODUCTION

Investigations of liquids and glasses by Small-Angle X-ray Scattering (SAXS) usually address the characterization of physical heterogeneity, e.g., dispersed nanoparticles or pores. Besides, SAXS provides quantitative data on local density fluctuations. While early research in this field focused on polymers, the technique was successfully adapted for the characterization of inorganic glasses (Pierre et al., 1972; Rathje and Ruland, 1976; Fischer and Dettenmaier, 1978; Wiegand and Ruland, 1979; Golubkov et al., 1980; Roe and Curro, 1983; Tanabe et al., 1984): spatial density fluctuations are a universal feature of glassy materials. For example, fluctuations in chemical composition may be caused by the presence of different chemical compounds with non-random (selective) bonding such as introduced by Greaves as an essential feature of the Modified Random Network

Model for glass structure (Greaves et al., 1981; Greaves, 1985). Physical fluctuations such as in network topology manifests in variations within the atomic arrangement, e.g., local network rigidity or packing density. The latter may depend on the thermal history of the glass, for example, quenching rates (Levelut et al., 2002, 2005, 2007; Brüning and Cottrell, 2003; Watanabe et al., 2003; Brüning et al., 2005, 2007) or pressure (Reibstein et al., 2011; Cornet et al., 2019). These frozen-in fluctuations typically occur at nanometer scale. Their assessment provides useful insight at the intermediate- to long-range structural characteristics of glasses (Greaves et al., 2008). As such density fluctuations are not strictly defined in shape or size (Golubkov, 1996; Bakai and Fischer, 2004; Ozhovan, 2006; Huang et al., 2018), they do not cause distinct, sharp scattering signals. Instead, their presence manifests in the overall scattering intensity at low scattering angles q , i.e., the extrapolated SAXS intensity to zero scattering angle $I(0)$.

In particular for metallic glasses, significant efforts have been undertaken in order to relate the occurrence of structural heterogeneity to mechanical behavior. This draws on the understanding of plastic flow in these materials, where localized shear transformation zones (STZs) are a primary factor in overall material deformation [e.g., (Yang et al., 2010; Huo et al., 2013; Li et al., 2015; Limbach et al., 2017; Zhu et al., 2018; Hilke et al., 2019)]. For inorganic glasses, the understanding of structural heterogeneity in the context of mechanical behavior remains less developed and mostly phenomenological, e.g., for material response to (nano)indentation (Benzine et al., 2018a; Poletto Rodrigues et al., 2019) or scratching (de Macedo et al., 2018; Sawamura and Wondraczek, 2018; Sawamura et al., 2019). In such experiments, the structural consequence of deformation is typically studied by well-established *ex-situ* (post-deformation) vibrational spectroscopy (Perriot et al., 2006; Koike and Tomozawa, 2007; Deschamps et al., 2011; Kassir-Bodon et al., 2012; Kato et al., 2012; Tran et al., 2012; Yoshida et al., 2012; Winterstein-Beckmann et al., 2014a,b; Januchta et al., 2017; Kilymis et al., 2017) and related to numerical stress field analysis (Kermouche et al., 2008; Gadelrab et al., 2012; Bruns et al., 2017, 2020a,b; Molnár et al., 2017). However, such an approach has various shortcomings. It provides only indirect information on the deformation process; transient (non-permanent) effects must be studied *in-situ* (Yoshida et al., 2019; Gerbig and Michaels, 2020). Longer-range structural information requires vibrational spectroscopy in the THz regime, which is still a challenge to do *in-situ* (Benzine et al., 2018b).

Here, we report on using Small-Angle X-ray Scattering with a customized nanoindentation set-up to evaluate the short- as well as intermediate- to long-range structural response of vitreous silica during loading with a sharp, wedge-shaped diamond indenter. For mapping experiments, we employ the P03 beamline at the German Synchrotron Facility DESY at PETRA III (Krywka et al., 2013; Gamcová et al., 2016; Zeilinger et al., 2016), offering low spot size and low beam opening angle for 2-dimensional mapping at a lateral resolution of about 1 μm .

MATERIALS AND METHODS

Commercial-grade vitreous silica (Herasil, Heraeus Quarzglas GmbH & Co. KG) was used for this study. The glass specimen was initially cut into a rectangular slice of 13 mm length and 3 mm height. All sides were polished to optical grade, with plane-parallel opposing faces. Afterwards, the specimen thickness was gradually reduced down to 467 μm to account for the transmission requirements of the scattering experiment. The glass specimen was glued on one side to the sample holder using a thermoplastic polymer (Crystal bond, Aremco Products Inc.), with the upper 1 mm being free-standing to avoid shadowing effects in the SAXS experiments (schematic drawing in **Supplementary Figure 1**).

Small-Angle X-ray Scattering (SAXS) experiments were carried out at the Nanofocus Endstation of the P03 beamline at PETRA III synchrotron, DESY, Hamburg, Germany (Krywka et al., 2012), using monochromatic X-rays with an energy of 15 keV. The beam was focused by a set of elliptical mirrors to achieve a beam size of 800 nm and an opening angle of 0.002 rad. A 2D detector (Dectris Pilatus 1M) with a detector field of 168.7 \times 179.4 mm^2 was positioned at a distance of 750 mm behind the sample. The scattering vector q was calibrated using silver behenate. The direct beam was detected by means of a semi-transparent beamstop, which was made of multiple layers of a thin silver foil up to a total nominal thickness of 330 μm .

The indentation set-up at P03 is realized with a multi-stage motor stack, which enables precise alignment of the indenter tip and the sample with six geometric degrees of freedom ($x, y, z, \chi, \phi, \vartheta$) and the movement of the whole relative to the X-ray beam for spatially resolved SAXS data acquisition (schematic drawing in **Supplementary Figure 1**). The scattering contribution is accumulated through the specimen thickness. Thus, a sharp wedge-shaped diamond indenter tip (Synton-MDP Inc.) with a length of 490 μm and an opening angle of 60° was used. A careful alignment procedure of beam and tip as well as sample to beam was carried out. This is to provide a homogeneous strain distribution along the beam path through the sample and to prevent the averaging-out of structural changes. However, the surface topography of the sample itself introduced averaging effects, which results in not quantitative comparable loading conditions (see below). Within the indentation set-up a frame decouples the sample positioning motors from the indenter tip. A stepwise increase of the load is achieved by moving the glass specimen upwards against the indenter tip. The applied load P was monitored by means of a capacitive force sensor (Kistler Instrumente GmbH) with a sensitivity of 10.55 pC/N, attached to the indenter tip. The maximum load must be limited to ~ 3 N due to the low load-tolerance of the hexapods and the piezoelectric positioners used. Two independent loadings were carried out. For indent 1 an initial maximum load of circa 2.4 N and for indent 2 an initial maximum load of circa 2.7 N were applied. The contact situation was checked by *post-mortem* analysis with wide-field confocal optical microscopy (Smartproof 5, Zeiss with a nominal lateral resolution of $(0.13 \pm 0.1) \mu\text{m}$ and a nominal accuracy in depth with $\pm 0.1 \mu\text{m}$ for the C Epiplan-APOCHROMAT

50 × /0.95 objective). **Figure 1** images the resulting imprints. Please note the curvature of the sample with a flattening and rounding of the face edges due to the manual preparation of the glass slides (U-shape in cross section). This results in gradually decreasing imprint depths, from ~300 nm in the center of the sample to ~60 nm toward the edges. The mean depth for indent 1 is ~175 nm and for indent 2 ~150 nm. This, in turn, implies different contact situations for the two indents, such that indent 2 exhibits an average lower indentation depth during loading, despite the higher maximum load recorded by the capacitive force sensor, which must be considered when comparing the SAXS data of indent 1 and 2. SAXS data were collected in transmission mode for the pristine sample, after loading, as well as after unloading. In each indentation experiment, a 2D SAXS map with step widths of 2 μm in horizontal *x*- and 1 μm in vertical *y*-direction relative to the indenter tip, covering a total area of ~12 × 22 μm², was acquired (refer to schematic drawing in **Supplementary Figure 1**). The scattered photons were accumulated for 60 s at each spot. During the accumulation of the SAXS data (~4.5 h for each imprint) a load decrease to ~2.2 N (indent 1) and ~2.4 N (indent 2), respectively, were observed. This decrease can primarily be attributed to relaxation processes occurring during the time of the SAXS measurement. Recent studies have shown that indentation relaxation in the order of ~10 % is likely to happen for such a period of time (Baral et al., 2019).

Data processing was carried-out using the software FIT2D (Hammersley et al., 1996). Each detector image was carefully checked before evaluation. No anisotropy effect due to an inhomogeneous deformation from an inclined diamond wedge or damage of the sample could be detected. In a first step, each detector image was masked to eliminate areas such as the beamstop, dead pixels, detector segments, or scattering and reflection contributions from the diamond indenter tip or sample surface. The data were then integrated azimuthally to generate curves of scattering intensity *I* as a function of scattering angle or scattering vector *q*. To extract information on the direct transmission, the beamstop area was selected and the intensity values of each pixel were summed-up. The scattering curves were normalized for the incident intensity decay of the PETRA III X-ray beam and their respective transmission value and thickness. Due to the beamstop located close to the detector, a large contribution from air scattering superimposes the low-angle scattering of the glass. In order to extract the scattering originating from the sample, multiple empty measurements (no sample installed, same set-up and measurement conditions) were collected and used to normalize the transmission scaled scattering intensities.

The stress field beneath the indenter tip was simulated via Finite Element Analysis using the software package (Abaqus 2016 Online Documentation, 2015). The indentation process was modeled according to previous reports (Bruns et al., 2017, 2020a,b) using a friction coefficient of 0.15 as suggested in literature (Johnson, 1970). The wedge-shaped indenter tip was approximated with a 2D representation, using the experimental tip area function as reference. All material parameters were assumed to represent isotropic and rate-insensitive room temperature values. A Young's modulus of 70 GPa and a Poisson's

ratio of 0.18 were used for vitreous silica (Limbach et al., 2014). The plastic material response was modeled using the cap section of Drucker-Prager-Cap plasticity to replicate the elliptical yield surface of vitreous silica (Kermouche et al., 2008). In this context a yield strength under pure shear of 7.5 GPa and a hydrostatic yield strength of 8 GPa were assumed. Sigmoidal densification hardening was implemented based on experimental diamond anvil cell data from literature (Rouxel et al., 2008; Deschamps et al., 2012; Sonnevile et al., 2012). Details on this procedure are reported elsewhere (Bruns et al., 2017, 2020b).

RESULTS

Spatially Resolved *in-situ* Small-Angle X-Ray Scattering

The comparably short sample to detector distance in the SAXS set-up allowed to observe the First Sharp Diffraction Peak (FSDP, also refer to **Supplementary Figure 3**). Its position relative to the sample surface and the indenter tip is shown in **Figure 2** for the two loadings (**Figures 2A,C**), together with the respective maps after unloading (**Figures 2B,D**). The indentation center (indenter tip) is located at $(x,y) = (0,0)$. As we expect a symmetric indentation profile, in order to reduce the required scanning time, only one half the deformation field was captured. The FSDP maximum is located around $q_{\text{FSDP}} = 15.2 \text{ nm}^{-1}$, in good accordance with literature (Warren et al., 1936; Elliott, 1991; Brüning and Cottrell, 2003). A rather small deviation of $\pm 0.1 \text{ nm}^{-1}$ was found within the bulk glass sample. Below the indenter tip, the FSDP is shifted toward higher scattering angles by about 0.6 nm^{-1} . As only half of the indent was mapped, a possible misalignment of the scan field cannot fully be excluded. Nevertheless, from the results presented in **Figure 2A** we can conclude that the position of the FSDP for indent 1 is affected within an area extending to at least 4 μm in lateral dimension from the loading axis and ~7 μm in depth.

The FSDP analysis shown in **Figure 2** indicates mostly elastic (reversible) effects. The complementary *post-mortem* inspection of the indented area by confocal optical microscopy revealed the creation of permanent imprints of about $1.5 \pm 0.3 \mu\text{m}$ in width (see **Figure 1**). Thus, not only elastic deformation, but also inelastic deformation in terms of either shear flow and/or permanent densification occurred during the experiment, which agrees with the expected indentation response of vitreous silica. The spatial resolution of the SAXS mappings is too low to resolve the residual imprint. Additionally, the obtained SAXS data results from a longitudinal view parallel to the wedge axis; hence, it integrates over any variations in indentation depth (which are different for both indents). The quantitative comparison of both indents shows obvious differences. Despite the nominal higher maximum load recorded for indent 2, a smaller FSDP shift as well as a more blurred shape of the stressed region can be noted in comparison to indent 1.

The further analysis of the SAXS data is based on the diffuse scattering level at low scattering angles, which represents the amplitude of electron density fluctuations (AEDF) in liquids and glasses (Porod, 1982). Since the investigated glass is pure

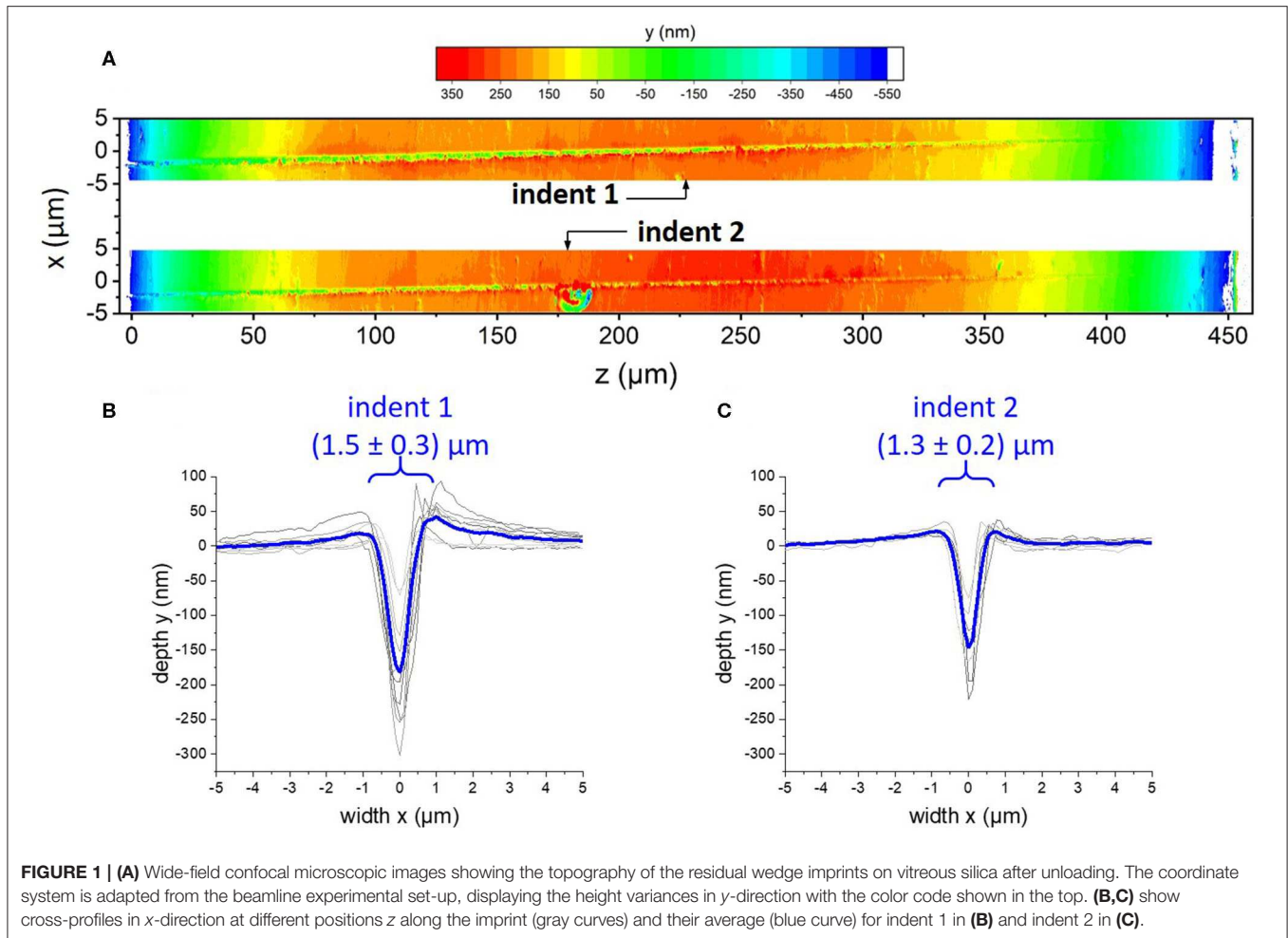
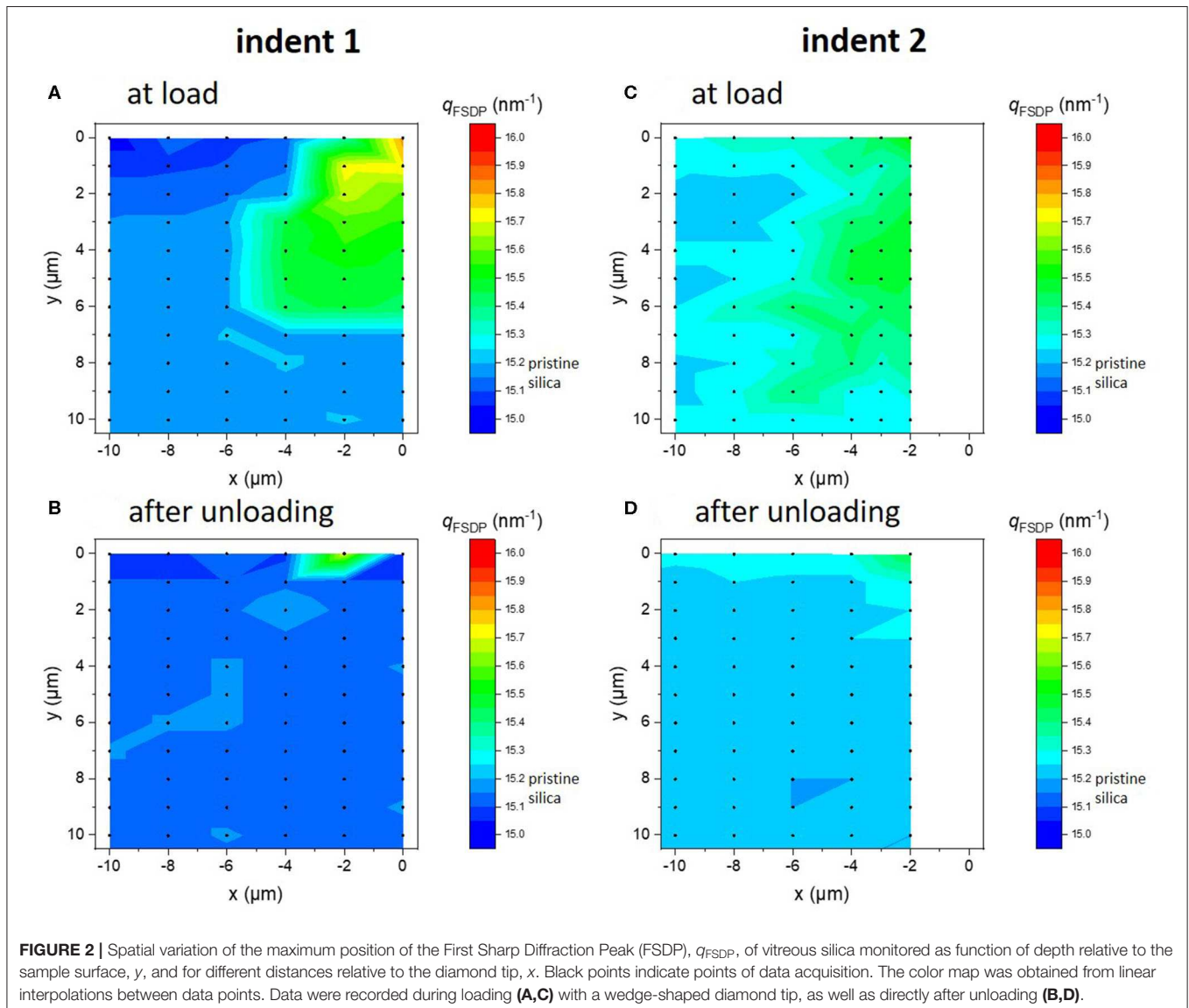


FIGURE 1 | (A) Wide-field confocal microscopic images showing the topography of the residual wedge imprints on vitreous silica after unloading. The coordinate system is adapted from the beamline experimental set-up, displaying the height variances in y -direction with the color code shown in the top. **(B,C)** show cross-profiles in x -direction at different positions z along the imprint (gray curves) and their average (blue curve) for indent 1 in **(B)** and indent 2 in **(C)**.

SiO_2 , changes of the AEDF upon deformation are only related to physical heterogeneity (no chemical fluctuations) (Levelut et al., 2002, 2005, 2007; Reibstein et al., 2011). In the present experiment, the AEDF reflects stress-induced modifications of the topological heterogeneity of the silica network *in-situ*. The scattering intensity at zero angle, $I_0 = I(q = 0)$, is employed as a measure of the low-angle scattering level. To extrapolate to I_0 , the scattering data obtained from the interval of $\sim 1.7 < q < 2.7 \text{ nm}^{-1}$ were linearized by plotting $\ln[I(q)]$ over q^2 ; I_0 was deduced from the intersection of a fitted straight line with the y -axis (Tanabe et al., 1984). This procedure is illustrated in **Supplementary Figure 3**. The absolute value of I_0 can vary depending on the chosen fitting range due to interference from the low-angle tail of the FSDP (Levelut et al., 2002). Data interpretation is therefore made under the assumption that the influence of the low angle scattering tail of the FSDP is equal for all data points in the chosen fitting range. The extrapolated values were normalized to the I_0^{bulk} of the pristine, bulk glass specimen. Data obtained in this way are presented in **Figure 3** as functions of the distance from the specimen surface in y -direction for various

distances x relative to the loading axis. A two-dimensional representation is provided exemplarily for indent 2 in the **Supplementary Figures S2C,D**.

When comparing the variation of the AEDF under load (**Figures 3A,C**) and after unloading (**Figures 3B,D**), it is obvious that the presence of a local stress field strongly influences the level of scattering at low angles, whereas the data after unloading indicate much less variation (circa $\pm 1\%$). The data recorded under load indicate for both indents a decrease in I_0 during indentation. Although the applied loads are relatively close, some differences are seen in their comparison, probably indicating the accuracy and reproducibility of the present method. This observation was already expected from the different topography of the imprints (see **Figure 1**). At indent 1 (**Figure 3A**), the normalized scattering intensity is consistently reduced by about 3–4% at distances up to $8 \mu\text{m}$ relative to the loading axis and for the full measurement depths down to $y = 21 \mu\text{m}$. In the vicinity of the indenter tip ($x = 0 \mu\text{m}$) the reduction in the normalized scattering intensity increases gradually down to a depth of $\sim 10 \mu\text{m}$. In a distance of $x = -10 \mu\text{m}$ from the indent center, no variations are found



in the AEDF. An overall smaller reduction of the normalized scattering intensity by $\sim 2\%$ (**Figure 3C**) is observed for indent 2 with the nominal higher peak load. However, this corresponds well to the overall smaller deformation (see **Figure 1C**). The aforementioned reduced normalized scattering intensity at the indent center is not reproduced. The scattering intensity rather seems to increase with increasing depth and would presumably reach the bulk value at a depth of about $27\ \mu\text{m}$. The depth profiles recorded at larger distances from the indenter tip all scatter within a narrow interval of $\pm 1\%$ and thus are not significantly influenced by the presence of the local stress field. It is nevertheless worth noting, that the data recorded down to depths of $\sim 3\text{--}4\ \mu\text{m}$ display strong scattering and exhibit large positive values.

Characterization of the Magnitude and Directionality of the Stress Field by FEA

Finite Element Analysis (FEA) was carried out in order to quantify the stress field below the indentation, using the geometry of the wedge-shaped diamond indenter tip as an input parameter in the 2D analysis. The simulations were performed under displacement control, until a similar residual indentation depth as found in the experiments was achieved. **Figure 4** depicts the von Mises equivalent stress (defined as J_2 , second invariant of stress deviator), the hydrostatic stress component p (defined as $\rho = -\sigma_{ii}/3$) as well as the densification (given as the volumetric inelastic strain) at maximum indentation depth under load. The von Mises equivalent stress $\sigma_{\text{equ.Mises}}$ in **Figure 4A** reveals a symmetric, ellipsoidal-shaped distribution with a radius of about

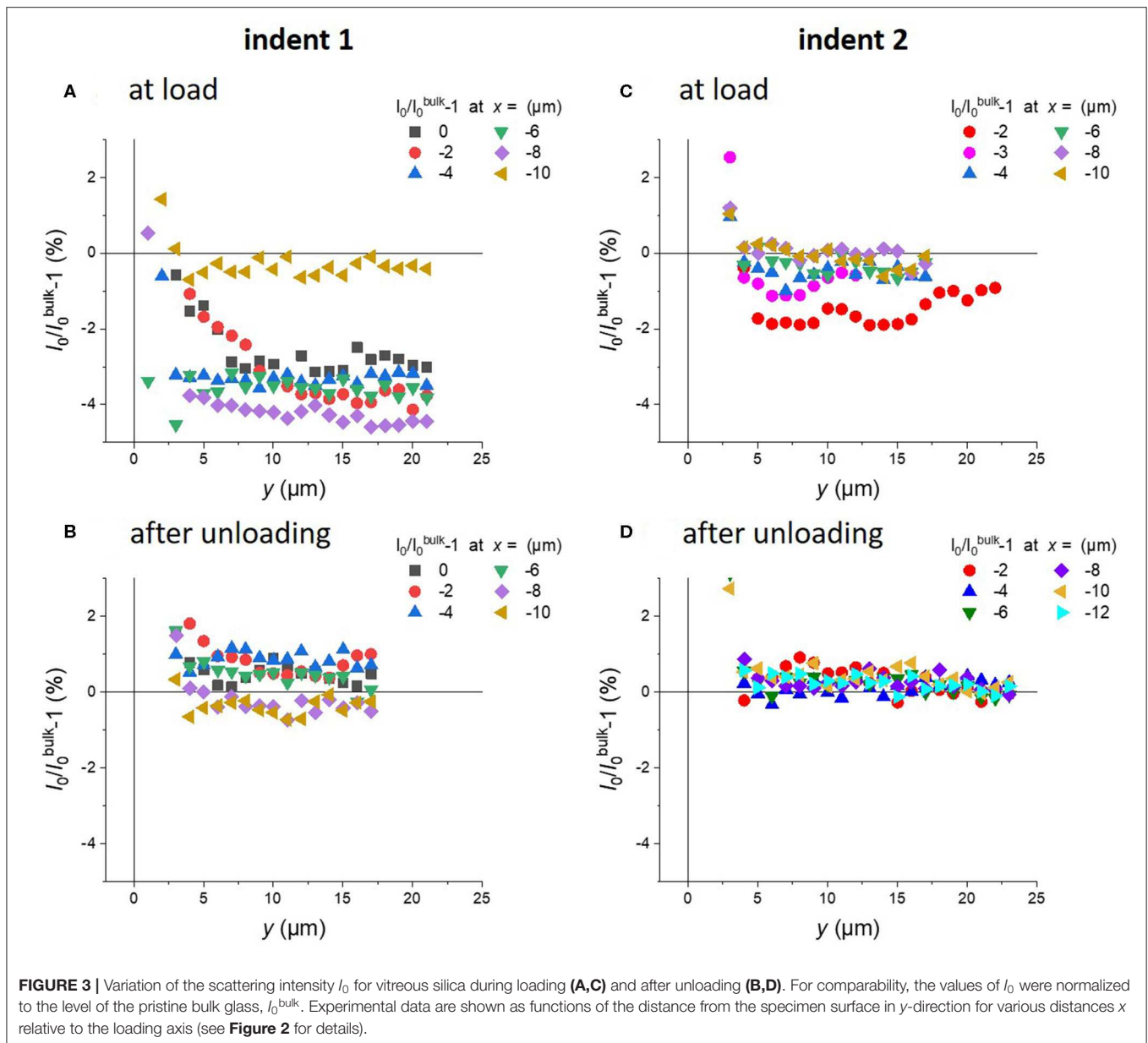


FIGURE 3 | Variation of the scattering intensity I_0 for vitreous silica during loading (A,C) and after unloading (B,D). For comparability, the values of I_0 were normalized to the level of the pristine bulk glass, I_0^{bulk} . Experimental data are shown as functions of the distance from the specimen surface in y -direction for various distances x relative to the loading axis (see **Figure 2** for details).

12 μm . Highest stresses occur directly at the indenter tip with a maximum of $\sigma_{\text{equ.Mises}} = 7.5$ GPa, according to the employed yield criterion. The hydrostatic stress field below the indenter is much smaller in dimension, but exhibits a similar shape as the von Mises stress field. It extends laterally up to $x \sim -5$ μm , whereas in depth a non-zero pressure stress is still calculated for $y = 8$ μm . The shear stress together with the hydrostatic pressure component induces a gradual densification in the plastic zone with a maximum of $\sim 16\%$ at the indent center (**Figure 4C**, inset).

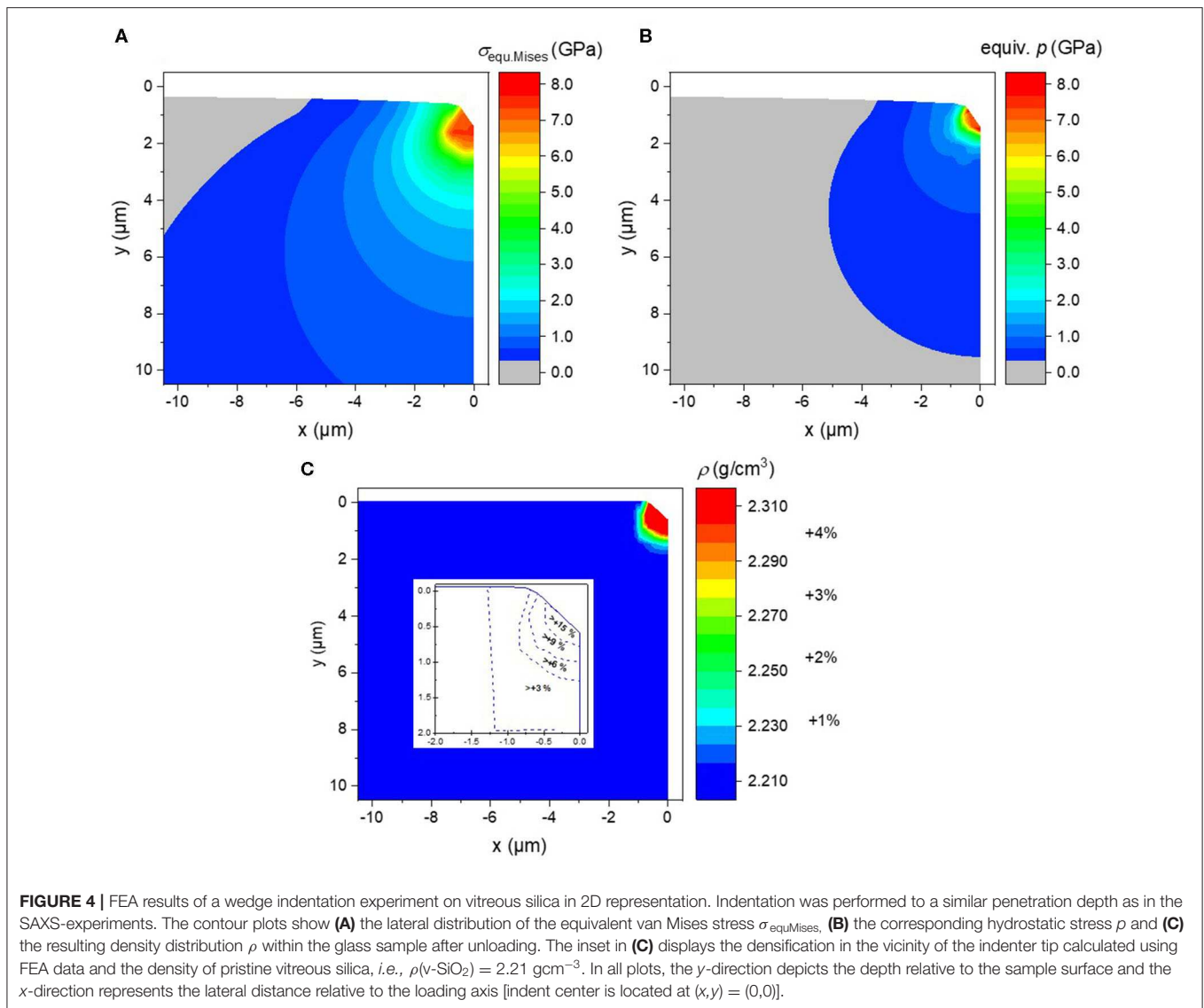
After unloading, a permanent imprint with a width of ~ 2 μm and a depth of ~ 0.7 μm is formed on the glass surface (**Figure 4C**). The permanent densification, however, only occurs within a small region which corresponds roughly to the direct contact zone. It spreads until $x \sim -1.5$ μm in width

and $y \sim 2$ μm in depth. The densification (**Figure 4C**) was calculated based on the density of pristine vitreous silica, i.e., $\rho(\text{v-SiO}_2) = 2.21$ gcm^{-3} , and the density distribution as derived from FEA.

DISCUSSION

Short- to Intermediate-Range Structural Response of Vitreous Silica to Indentation

The FSDP in glasses originates from local variations in structural order. In vitreous silica the FSDP reflects the distribution of the SiO_4 inter-tetrahedral distances and Si-O-Si bond angles (Elliott, 1991; Brüning and Cottrell, 2003). The correlated real

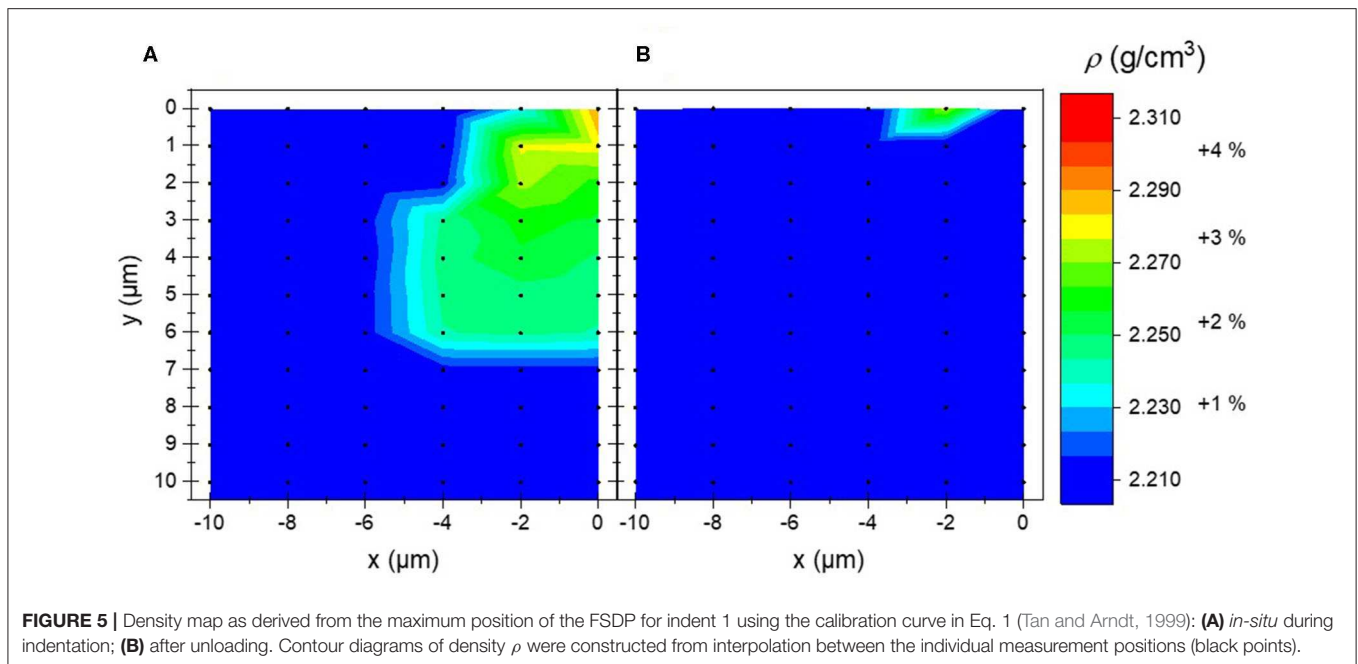


space length, $d = 2\pi/q$, for the intensity maximum of the pristine bulk glass calculates to $\sim 4.1 \text{ \AA}$. The observed positive shift of the FSDP maximum (**Figures 2A,C**) indicates a decrease of the real space length during loading, and thus, a decrease in the inter-tetrahedral distances and bond angles. This observation is in agreement with similar reports on densified glasses (Elliott, 1991). When the structure compacts, distances and bond angles decrease. According to Tan and Arndt (Tan and Arndt, 1999), the maximum position of the FSDP in vitreous silica follows a linear trend with the glass density via the following empirical relation:

$$\rho = 1.621 + 41.9(1/d^3) \quad (1)$$

Using the above expression and the results from the FSDP (**Figures 2A,C**), a density map for indent 1 *in-situ* under applied load (**Figure 5A**) and after unloading (**Figure 5B**) is constructed.

The densification during loading reaches its maximum of about 3 % in the vicinity of the indenter tip and the affected area extends up to roughly $x \sim 6 \mu\text{m}$. This compares well with the FEA results (**Figure 4B**). When releasing the stress, the major part of the FSDP variation is recovered, leaving only a slight trace of residual modification (**Figure 5B**). At first glance, this observation appears to be contradictory to the FEA, which predicts a maximum densification of about 15% directly below the indenter tip (**Figure 4C**). However, the spatial resolution of the X-ray scattering experiment does presently not allow for further interpretation. The SAXS investigation is not only affected by the curvature of the surface (**Figure 1A**), but also strongly influenced by a signal averaging effect over a structural gradient at the imprint center (Bruns et al., 2020b). Both FEA and SAXS, however, agree in that the size of the permanent densified material below the indent is confined to a local area of $\sim 2 \times 2 \mu\text{m}^2$ in dimension.



Evaluation of Structural Heterogeneity in Vitreous Silica During Indentation

The densification of about 3% during loading (Figure 5A), which was determined from the positive shift of the FSDP to higher scattering angles (Figure 2A), coincides very well with the relative reduction of the AEDF compared to the bulk value of about 3–4% (Figure 3A). It appears that the local stress-field produced by the wedge-shaped diamond indenter tip induces comparable extents of structural modification across all length scales (as reflected by the changes in the position of the FSDP and by the variations in the AEDF, which are directly correlated to the longer-range structural heterogeneity on the scale of a few nanometers). Under load, the overall AEDF was reduced and thus, the material became more homogeneous. Interestingly, while structural variations at short- to intermediate-length scales are confined within a narrow volume in the vicinity of the indent center and for depths down to $\sim 6.5 \mu\text{m}$ (Figure 2, Figure 5A, respectively), it appears that modifications in the topological heterogeneity as derived from the AEDF (Figure 3) are achieved in a considerably larger volume spreading to about $8 \mu\text{m}$ in radial direction (x) and more than $22 \mu\text{m}$ in depth (y). We note, that similar observations were made for indent 2 (see Supplementary Figure 2), although the different loading conditions impede a quantitative comparison between both indents. The size of the AEDF field corresponds well to the FEA equivalent von Mises stress field beneath the indenter tip (Figure 4A), whereas the extent of the FSDP field corresponds well to the FEA isostatic equivalent pressure stress field (Figure 4B). We therefore conclude that the reduction of the AEDF and the shift in the FSDP are induced by different stress components and that they are not necessarily directly correlated to each other. On high

pressure derived glasses it has been recognized that pressure-induced modifications at the short-range structural order may not be sufficient to explain the variations in density (Wondraczek and Behrens, 2007; Wondraczek et al., 2007; Wu et al., 2009), but the increase in long-range structural homogeneity has a major contribution as well (Reibstein et al., 2011). These observations indicate that the topological heterogeneity at longer-range is more sensitive to the shear stress component than the short- to intermediate-range structure of a glass. This becomes evident from the good correlation between the affected area in the AEDF analysis and the FEA equivalent von Mises stress field, which contains shear stress components. It should be noted, that both the FSDP shift and the reduction of the AEDF only persist upon loading, i.e., when the glass is exposed to the stress field of the indenter tip. Major parts of the glassy structure relax without permanent structural modifications upon the relief of the stresses at unloading.

CONCLUSION

In summary, we presented *in-situ* SAXS as a complementary method to study structural modification induced by local material deformation on intermediate length scale. Such investigations allow for relating macroscopic observations (e.g., material compaction or stress fields) to structural heterogeneity. They may help to elucidate the discrepancies between observations made on short (molecular) length scale and physical property variations toward an improved understanding of the reactions which lead to glass deformation. In vitreous silica subjected to wedge indentation, structural motives with a correlation length of $\sim 0.4 \text{ nm}$ show permanent, irreversible

changes, whereas the longer-range structure (≥ 1 nm) fully recovers upon stress release. From the comparison of the affected region with FEA of the stress field, we found that shear and non-permanent densification seem to act as the primary factors on the longer-range structure. This should be investigated systematically at higher load and in glass systems with higher Poisson's ratio, where shear is more pronounced over pure densification. For this, it will be necessary to optimize the indentation set-up at the beamline to increase load tolerance and frame stiffness as well as to perform experiments with higher scanning resolution (i.e., spatial resolution).

DATA AVAILABILITY STATEMENT

The datasets generated for this study are available on request to the corresponding author.

AUTHOR CONTRIBUTIONS

SF and LW conceived of the study. The experimental design, the conduction of the SAXS experiment and data interpretation were made by SF, GM, RL, and CK. RL performed the mechanical analysis and stiffness calibration. SB and KD set and performed Finite Element Analysis. All authors participated in manuscript writing, revision, and final approval.

REFERENCES

- Abaqus 2016 Online Documentation (2015). *Dassault Systèmes*. Available online at: <http://abaqus.software.polimi.it/v2016/> (accessed March 5, 2020).
- Bakai, A. S., and Fischer, E. W. (2004). Nature of long-range correlations of density fluctuations in glass-forming liquids. *J. Chem. Phys.* 120, 5235–5252. doi: 10.1063/1.1648300
- Babal, P., Guillonnet, G., Kermouche, G., Bergheau, J. M., and Loubet, J. L. (2019). A new long-term indentation relaxation method to measure creep properties at the micro-scale with application to fused silica and PMMA. *Mech. Mater.* 137:103095. doi: 10.1016/j.mechmat.2019.103095
- Benzine, O., Bruns, S., Pan, Z., Durst, K., and Wondraczek, L. (2018). Local deformation of glasses is mediated by rigidity fluctuation on nanometer scale. *Adv. Sci.* 5:1800916. doi: 10.1002/adv.201800916
- Brüning, R., and Cottrell, D. (2003). X-ray and neutron scattering observations of structural relaxation of vitreous silica. *J. Non Cryst. Solids* 325, 6–15. doi: 10.1016/S0022-3093(03)00318-1
- Brüning, R., Levelut, C., Faivre, A., LeParc, R., Simon, J. P., Bley, F., et al. (2005). Characterization of the glass transition in vitreous silica by temperature scanning small-angle X-ray scattering. *Europhys. Lett.* 70, 211–217. doi: 10.1209/epl/i2004-10481-1
- Brüning, R., Levelut, C., Parc, R. L., Faivre, A., Semple, L., Vallee, M., et al. (2007). Temperature scanning small angle x-ray scattering measurements of structural relaxation in type-III vitreous silica. *J. Appl. Phys.* 102, 083535–083539. doi: 10.1063/1.2799940
- Bruns, S., Johanns, K. E., Rehman, H. U. R., Pharr, G. M., and Durst, K. (2017). Constitutive modeling of indentation cracking in fused silica. *J. Am. Ceramic Soc.* 100, 1928–1940. doi: 10.1111/jace.14734
- Bruns, S., Petho, L., Minnert, C., Michler, J., and Durst, K. (2020a). Fracture toughness determination of fused silica by cube corner indentation cracking and pillar splitting. *Mater. Des.* 186:108311. doi: 10.1016/j.matdes.2019.108311

FUNDING

The authors gratefully acknowledge the Deutsches Elektronen-Synchrotron (DESY, Hamburg, Germany) a member of the Helmholtz Association HGF for assigning beamtime (I-20150108, I-20140502) and supporting travel expenses. This project is funded through the priority program 1594 of the German Science Foundation by the starting-ramp funding through grant no. WO1220/8-1 and project grant nos. DU424/8-2 and FU1018/1-2.

ACKNOWLEDGMENTS

We acknowledge DESY (Hamburg, Germany), a member of the Helmholtz Association HGF, for the provision of experimental facilities. Major parts of this research were carried out at PETRA III at P03 MINAXS. We thank OSIM technician Christian Zeidler for his help and support during confocal microscopy data acquisition, our colleague Aaron Reupert and our former students Florian Baumgardt and Christoph Dittmann for assistance during beamtime experiments.

SUPPLEMENTARY MATERIAL

The Supplementary Material for this article can be found online at: <https://www.frontiersin.org/articles/10.3389/fmats.2020.00173/full#supplementary-material>

- Bruns, S., Uesbeck, T., Tarragó Aymerich, M., Fuhrmann, S., Wondraczek, L., de Ligny, D., et al. (2020b). Indentation densification of fused silica assessed by raman spectroscopy and constitutive finite element analysis. *J. Am. Ceramic Soc.* 103, 3076–3088. doi: 10.1111/jace.17024
- Cornet, A., Martinet, C., Martinez, V., and Ligny, D. (2019). Evidence of polyamorphic transitions during densified SiO₂ glass annealing. *J. Chem. Phys.* 151:164502. doi: 10.1063/1.5121534
- de Macedo, G., Sawamura, S., and Wondraczek, L. (2018). Lateral hardness and the scratch resistance of glasses in the Na₂O–CaO–SiO₂ system. *J. Non Cryst. Solids* 492, 94–101. doi: 10.1016/j.jnoncrysol.2018.04.022
- Deschamps, T., Kassir-Bodon, A., Sonnevile, C., Margueritat, J., Martinet, C., de Ligny, D., et al. (2012). Permanent densification of compressed silica glass: a Raman-density calibration curve. *J. Phys. Condensed Matter* 25:025402. doi: 10.1088/0953-8984/25/2/025402
- Deschamps, T., Martinet, C., Bruneel, J. L., and Champagnon, B. (2011). Soda-lime silicate glass under hydrostatic pressure and indentation: a micro-Raman study. *J. Phys. Condensed Matter* 23:035402. doi: 10.1088/0953-8984/23/3/035402
- Elliott, S. R. (1991). Origin of the first sharp diffraction peak in the structure factor of covalent glasses. *Phys. Rev. Lett.* 67, 711–714. doi: 10.1103/PhysRevLett.67.711
- Fischer, E. W., and Dettenmaier, M. (1978). Structure of polymeric glasses and melts. *J. Non Cryst. Solids* 31, 181–205. doi: 10.1016/0022-3093(78)90104-7
- Gadelrab, K. R., Bonilla, F. A., and Chiesa, M. (2012). Densification modeling of fused silica under nanoindentation. *J. Non Cryst. Solids* 358, 392–398. doi: 10.1016/j.jnoncrysol.2011.10.011
- Gamcová, J., Mohanty, G., Michalik, Š., Wehrs, J., Bednarčík, J., Krywka, C., et al. (2016). Mapping strain fields induced in Zr-based bulk metallic glasses during in-situ nanoindentation by X-ray nanodiffraction. *Appl. Phys. Lett.* 108, 031907. doi: 10.1063/1.4939981
- Gerbig, Y. B., and Michaels, C. A. (2020). In-situ Raman spectroscopic measurements of the deformation region in indented glasses. *J. Non Cryst. Solids* 530:119828. doi: 10.1016/j.jnoncrysol.2019.119828

- Golubkov, V. V. (1996). Features of structure and its relaxations in alkali borate glasses. *Glass Phys. Chem.* 22, 186–195.
- Golubkov, V. V., Vasilevska, T. N., and Porai-Koshits, E. A. (1980). SAXS study of the structure of glasses containing no modifying oxides. *J. Non Cryst. Solids* 38–39, 99–104. doi: 10.1016/0022-3093(80)90401-9
- Greaves, G. N. (1985). EXAFS and the structure of glass. *J. Non Cryst. Solids* 71, 203–217. doi: 10.1016/0022-3093(85)90289-3
- Greaves, G. N., Fontaine, A., Lagarde, P., Raoux, D., and Gurman, S. J. (1981). Local structure of silicate glasses. *Nature* 293, 611–616. doi: 10.1038/293611a0
- Greaves, G. N., Wilding, M. C., Kargl, F., and Hennes, L. (2008). Liquids, glasses, density fluctuations and low frequency modes. *Adv. Mat. Res.* 39–40, 3–12. doi: 10.4028/www.scientific.net/AMR.39-40.3
- Hammersley, A. P., Svensson, S. O., Hanfland, M., Fitch, A. N., and Hausermann, D. (1996). Two-dimensional detector software: from real detector to idealised image or two-theta scan. *High Press. Res.* 14, 235–248. doi: 10.1080/08957959608201408
- Hilke, S., Rösner, H., Geissler, D., Gebert, A., Peterlechner, M., and Wilde, G. (2019). The influence of deformation on the medium-range order of a Zr-based bulk metallic glass characterized by variable resolution fluctuation electron microscopy. *Acta Mater.* 171, 275–281. doi: 10.1016/j.actamat.2019.04.023
- Huang, B., Ge, T. P., Liu, G. L., Luan, J. H., He, Q. F., Yuan, Q. X., et al. (2018). Density fluctuations with fractal order in metallic glasses detected by synchrotron X-ray nano-computed tomography. *Acta Mater.* 155, 69–79. doi: 10.1016/j.actamat.2018.05.064
- Huo, L. S., Zeng, J. F., Wang, W. H., Liu, C. T., and Yang, Y. (2013). The dependence of shear modulus on dynamic relaxation and evolution of local structural heterogeneity in a metallic glass. *Acta Mater.* 61, 4329–4338. doi: 10.1016/j.actamat.2013.04.004
- Januchta, K., Youngman, R. E., Goel, A., Bauchy, M., Logunov, S. L., Rzoska, S. J., et al. (2017). Discovery of ultra-crack-resistant oxide glasses with adaptive networks. *Chem. Mater.* 29, 5865–5876. doi: 10.1021/acs.chemmater.7b00921
- Johnson, K. L. (1970). The correlation of indentation experiments. *J. Mech. Phys. Solids* 18, 115–126. doi: 10.1016/0022-5096(70)90029-3
- Kassir-Bodon, A., Deschamps, T., Martinet, C., Champagnon, B., Teisseire, J., and Kermouche, G. (2012). Raman mapping of the indentation-induced densification of a soda-lime-silicate glass. *Int. J. Appl. Glass Sci.* 3, 29–35. doi: 10.1111/j.2041-1294.2012.00078.x
- Kato, Y., Yamazaki, H., Yoshida, S., Matsuo, J., and Kanzaki, M. (2012). Measurements of density distribution around vickers indentation on commercial aluminoborosilicate and soda-lime silicate glasses by using micro Raman spectroscopy. *J. Non Cryst. Solids* 358, 3473–3480. doi: 10.1016/j.jnoncrysol.2012.04.035
- Kermouche, G., Barthel, E., Vandembroucq, D., and Dubujet, P. (2008). Mechanical modelling of indentation-induced densification in amorphous silica. *Acta Mater.* 56, 3222–3228. doi: 10.1016/j.actamat.2008.03.010
- Kilymis, D., Faivre, A., Michel, T., Peugeot, S., Delaye, J.-M., Delrieu, J., et al. (2017). Raman spectra of indented pristine and irradiated sodium borosilicate glasses. *J. Non Cryst. Solids* 464, 5–13. doi: 10.1016/j.jnoncrysol.2017.03.012
- Koike, A., and Tomozawa, M. (2007). IR investigation of density changes of silica glass and soda-lime silicate glass caused by microhardness indentation. *J. Non Cryst. Solids* 353, 2318–2327. doi: 10.1016/j.jnoncrysol.2007.04.006
- Krywka, C., Keckes, J., Storm, S., Buffet, A., Roth, S. V., Döhrmann, R., et al. (2013). Nanodiffraction at MINAXS (P03) beamline of PETRA III. *J. Phys. Conference Series* 425:072021. doi: 10.1088/1742-6596/425/7/072021
- Krywka, C., Neubauer, H., Priebe, M., Salditt, T., Keckes, J., Buffet, A., et al. (2012). A two-dimensional waveguide beam for X-ray nanodiffraction. *J. Appl. Crystallogr.* 45, 85–92. doi: 10.1107/S0021889811049132
- Levelut, C., Faivre, A., Le Parc, R., Champagnon, B., Hazemann, J. L., David, L., et al. (2002). Influence of thermal aging on density fluctuations in oxide glasses measured by small-angle X-ray scattering. *J. Non Cryst. Solids* 307–310, 426–435. doi: 10.1016/S0022-3093(02)01504-1
- Levelut, C., Faivre, A., Le Parc, R., Champagnon, B., Hazemann, J. L., and Simon, J. P. (2005). In situ measurements of density fluctuations and compressibility in silica glasses as a function of temperature and thermal history. *Phys. Rev. B* 72:224201. doi: 10.1103/PhysRevB.72.224201
- Levelut, C., Le Parc, R., Faivre, A., Brüning, R., Champagnon, B., Martinez, V., et al. (2007). Density fluctuations in oxide glasses investigated by small-angle X-ray scattering. *J. Appl. Crystallogr.* 40, 512–516. doi: 10.1107/S0021889807000507
- Li, W. D., Gao, Y. F., and Bei, H. B. (2015). On the correlation between microscopic structural heterogeneity and embrittlement behavior in metallic glasses. *Sci. Rep.* 5:15. doi: 10.1038/srep14786
- Limbach, R., Kosiba, K., Pauly, S., Kühn, U., and Wondraczek, L. (2017). Serrated flow of CuZr-based bulk metallic glasses probed by nanoindentation: role of the activation barrier, size and distribution of shear transformation zones. *J. Non Cryst. Solids* 459, 130–141. doi: 10.1016/j.jnoncrysol.2017.01.015
- Limbach, R., Poletto Rodrigues, B., and Wondraczek, L. (2014). Strain-rate sensitivity of glasses. *J. Non Cryst. Solids* 404, 124–134. doi: 10.1016/j.jnoncrysol.2014.08.023
- Molnár, G., Kermouche, G., and Barthel, E. (2017). Plastic response of amorphous silicates, from atomistic simulations to experiments – a general constitutive relation. *Mech. Mater.* 114, 1–8. doi: 10.1016/j.mechmat.2017.07.002
- Ozhovan, M. I. (2006). Topological characteristics of bonds in SiO₂ and GeO₂ oxide systems upon a glass-liquid transition. *J. Exp. Theor. Phys.* 103, 819–829. doi: 10.1134/S1063776106110197
- Perriot, A., vandembroucq, D., Barthel, E., Martinez, V., Grosvalet, L., Martinet, C., et al. (2006). Raman microspectroscopic characterization of amorphous silica plastic behavior. *J. Am. Ceramic Soc.* 89, 596–601. doi: 10.1111/j.1551-2916.2005.00747.x
- Pierre, A., Uhlmann, D. R., and Molea, F. N. (1972). Small-angle X-ray scattering study of glassy GeO₂. *J. Appl. Crystallogr.* 5, 216–221. doi: 10.1107/S0021889872009227
- Poletto Rodrigues, B., Limbach, R., Buzatto de Souza, G., Ebdorff-Heidepriem, H., and Wondraczek, L. (2019). Correlation between ionic mobility and plastic flow events in NaPO₃-NaCl-Na₂SO₄ glasses. *Front. Mater.* 6:128. doi: 10.3389/fmats.2019.00128
- Porod, G. (1982). “General theory,” in *Small Angle X-ray Scattering*, eds O. Glatter and O. Kratky. (London, UK: Academic Press), 17–51.
- Rathje, J., and Ruland, W. (1976). Density fluctuations in amorphous and semicrystalline polymers. *Colloid Polym. Sci.* 254, 358–370. doi: 10.1007/BF01384035
- Reibstein, S., Wondraczek, L., de Ligny, D., Krolkowski, S., Sirotkin, S., Simon, J. P., et al. (2011). Structural heterogeneity and pressure-relaxation in compressed borosilicate glasses by in situ small angle X-ray scattering. *J. Chem. Phys.* 134:204502. doi: 10.1063/1.3593399
- Roe, R. J., and Curro, J. J. (1983). Small-angle x-ray scattering study of density fluctuation in polystyrene annealed below the glass transition temperature. *Macromolecules* 16, 428–434. doi: 10.1021/ma00237a018
- Rouxel, T., Ji, H., Hammouda, T., and Moréac, A. (2008). Poisson’s ratio and the densification of glass under high pressure. *Phys. Rev. Lett.* 100:225501. doi: 10.1103/PhysRevLett.100.225501
- Sawamura, S., Limbach, R., Wilhelmy, S., Koike, A., and Wondraczek, L. (2019). Scratch-induced yielding and ductile fracture in silicate glasses probed by nanoindentation. *J. Am. Ceramic Soc.* 102, 7299–7311. doi: 10.1111/jace.16679
- Sawamura, S., and Wondraczek, L. (2018). Scratch hardness of glass. *Phys. Rev. Mater.* 2:092601. doi: 10.1103/PhysRevMaterials.2.092601
- Sonneville, C., Mermet, A., Champagnon, B., Martinet, C., Marguerit, J., de Ligny, D., et al. (2012). Progressive transformations of silica glass upon densification. *J. Chem. Phys.* 137:124505. doi: 10.1063/1.4754601
- Tan, C. Z., and Arndt, J. (1999). X-ray diffraction of densified silica glass. *J. Non Cryst. Solids* 249, 47–50. doi: 10.1016/S0022-3093(99)00245-8
- Tanabe, Y., Müller, N., and Fischer, E. W. (1984). Density fluctuation in amorphous polymers by small angle X-ray scattering. *Polym. J.* 16, 445–452. doi: 10.1295/polymj.16.445
- Tran, H., Clément, S., Vialla, R., Vandembroucq, D., and Rufflé, B. (2012). Micro-Brillouin spectroscopy mapping of the residual density field induced by Vickers indentation in a soda-lime silicate glass. *Appl. Phys. Lett.* 100:231901. doi: 10.1063/1.4725488
- Warren, B. E., Krutter, H., and Morningstar, O. (1936). Fourier analysis of X-ray patterns of vitreous SiO₂ and B₂O₃. *J. Am. Ceramic Soc.* 19, 202–206. doi: 10.1111/j.1151-2916.1936.tb19822.x
- Watanabe, T., Saito, K., and Ikushima, A. J. (2003). Fictive temperature dependence of density fluctuation in SiO₂ glass. *J. Appl. Phys.* 94, 4824–4827. doi: 10.1063/1.1608477
- Wiegand, W., and Ruland, W. (1979). “Density fluctuations and the state of order of amorphous polymers,” in *Anwendungsbezogene physikalische Charakterisierung von Polymeren, insbesondere im festen Zustand*, eds

- E.W. Fischer, F.H. Müller and R. Bonart. (Darmstadt: Steinkopff), 355–366. doi: 10.1007/BFb0117367
- Winterstein-Beckmann, A., Möncke, D., Palles, D., Kamitsos, E. I., and Wondraczek, L. (2014a). Raman spectroscopic study of structural changes induced by micro-indentation in low alkali borosilicate glasses. *J. Non Cryst. Solids* 401, 110–114. doi: 10.1016/j.jnoncrysol.2013.12.038
- Winterstein-Beckmann, A., Möncke, D., Palles, D., Kamitsos, E. I., and Wondraczek, L. (2014b). A Raman-spectroscopic study of indentation-induced structural changes in technical alkali-borosilicate glasses with varying silicate network connectivity. *J. Non Cryst. Solids* 405, 196–206. doi: 10.1016/j.jnoncrysol.2014.09.020
- Wondraczek, L., and Behrens, H. (2007). Molar volume, excess enthalpy, and prigogine-defay ratio of some silicate glasses with different (P,T) histories. *J. Chem. Phys.* 127:154503. doi: 10.1063/1.2794745
- Wondraczek, L., Sen, S., Behrens, H., and Youngman, R. E. (2007). Structure-energy map of alkali borosilicate glasses: effects of pressure and temperature. *Phys. Rev. B* 76:014202. doi: 10.1103/PhysRevB.76.014202
- Wu, J., Deubener, J., Stebbins, J. F., Grygarova, L., Behrens, H., Wondraczek, L., et al. (2009). Structural response of a highly viscous aluminoborosilicate melt to isotropic and anisotropic compressions. *J. Chem. Phys.* 131:104504. doi: 10.1063/1.3223282
- Yang, Y., Ye, J. C., Lu, J., Wang, Q., and Liaw, P. K. (2010). Revelation of the effect of structural heterogeneity on microplasticity in bulk metallic-glasses. *J. Mater. Res.* 25, 563–575. doi: 10.1557/JMR.2010.0058
- Yoshida, S., Nguyen, T. H., Yamada, A., and Matsuoka, J. (2019). In-situ raman measurements of silicate glasses during vickers indentation. *Mater. Trans.* 60, 1428–1432. doi: 10.2320/matertrans.MD201901
- Yoshida, S., Nishikubo, Y., Konno, A., Sugawara, T., Miura, Y., and Matsuoka, J. (2012). Fracture- and indentation-induced structural changes of sodium borosilicate glasses. *Int. J. Appl. Glass Sci.* 3, 3–13. doi: 10.1111/j.2041-1294.2011.00077.x
- Zeilinger, A., Todt, J., Krywka, C., Müller, M., Ecker, W., Sartory, B., et al. (2016). In-situ observation of cross-sectional microstructural changes and stress distributions in fracturing TiN thin film during nanoindentation. *Sci. Rep.* 6:22670. doi: 10.1038/srep22670
- Zhu, F., Song, S. X., Reddy, K. M., Hirata, A., and Chen, M. W. (2018). Spatial heterogeneity as the structure feature for structure-property relationship of metallic glasses. *Nat. Commun.* 9:7. doi: 10.1038/s41467-018-06476-8

Conflict of Interest: The authors declare that the research was conducted in the absence of any commercial or financial relationships that could be construed as a potential conflict of interest.

Copyright © 2020 Fuhrmann, de Macedo, Limbach, Krywka, Bruns, Durst and Wondraczek. This is an open-access article distributed under the terms of the Creative Commons Attribution License (CC BY). The use, distribution or reproduction in other forums is permitted, provided the original author(s) and the copyright owner(s) are credited and that the original publication in this journal is cited, in accordance with accepted academic practice. No use, distribution or reproduction is permitted which does not comply with these terms.